RSC Advances

PAPER

View Article Online
View Journal | View Issue

Cite this: *RSC Adv.*, 2024, **14**, 39804

Functionalization of 3D printed poly(lactic acid)/graphene oxide/β-tricalcium phosphate (PLA/GO/TCP) scaffolds for bone tissue regeneration application

Angela Sánchez-Cepeda, *[a] M. Carolina Pazos,[ab] Prieto-Abello Leonardo,[c] Silva-Cote Ingrid,[c] Luz Stella Correa-Araujo,[c] Chávez García María de Lourdes[d] and Ricardo Vera-Graziano[e]

The challenge of bone tissue regeneration implies the use of new advanced technologies for the manufacture of polymeric matrices, with 3D printing technology being a suitable option for tissue engineering due to its low processing cost, its simple operation and the wide use of biomaterials in biomedicine. Among the biopolymers used to obtain porous scaffolds, poly(lactic acid) (PLA) stands out due its mechanical and biodegradability properties, although its low bioactivity to promote bone regeneration is a great challenge. In this research, a 3D scaffold based on PLA reinforced with bioceramics such as graphene oxide (GO) and β-tricalcium phosphate (TCP) was designed and characterized by FTIR, XRD, DSC, SEM and mechanical tests. The *in vitro* biocompatibility, viability, and cell proliferation of the poly-L-lysine (POLYL) functionalized scaffold were investigated using Wharton Jelly mesenchymal stem cells (hWJ-MSCs) and confirmed by XPS. The incorporation of GO/TCP bioceramics into the PLA polymer matrix increased the mechanical strength and provided a thermal barrier during the fusion treatments that the polymeric material undergoes during its manufacturing. The results show that the functionalization of the scaffold with POLYL allows improving the cell adhesion, proliferation and differentiation of hWJ-MSCs. The resulting scaffold PLA/GO/TCP/POLYL exhibits enhanced structural integrity and osteogenic cues, rendering it a promising candidate for biomedical applications.

Received 13th August 2024
Accepted 3rd December 2024

DOI: 10.1039/d4ra05889e

rsc.li/rsc-advances

Introduction

Tissue engineering is a discipline of regenerative medicine that focuses on developing strategies to restore, maintain, or improve damaged tissues or organs by combining scaffolds, cells, and biologically active molecules, thus creating functional tissues.[1] This field of research has evolved with the development of 3D nanostructured biomaterials (artificial tissues), promoting specific interactions between cells and the scaffold, similar to those that occur during the restoration or replacement of damaged tissues. In this way, synthetic scaffolds will reduce invasive treatments with metallic orthopedic materials to treat complex and often chronic diseases that require two-step surgical interventions, the first step is to place the implant for fixation and the second to remove the metallic device after healing.[2,3] The Additive Manufacturing (AM) technique also called 3D printing, allows the development of complex, personalized structures, obtained in short processing times and low production costs. They are widely used in obtaining thermoplastic polymeric biomaterials reinforced with nanocomposites for applications of bioactive materials or scaffolds.[4,5]

Fused deposition modelling (FDM) is the most widely used AM process in the biomedical field.[4] With this technique, 3D pore microarchitectures are created from a computer-aided design (CAD) model by controlling the pore size, geometry, and interconnectivity.[6] These physical and mechanical properties favor the exchange of nutrients and cells,[7] promote cell viability and internal tissue growth.[6] Poly(lactic acid) (PLA) is one of the most used biopolymers in FDM, because it is

[a]*Facultad de Ciencias Básicas, Escuela de Posgrados, Universidad Pedagógica y Tecnológica de Colombia UPTC, Avda. Central del Norte, Vía Paipa, 150001 Tunja, Boyacá, Colombia. E-mail: angelapatricia.sanchez@uptc.edu.co*

[b]*Escuela de Ciencias Químicas, Facultad de Ciencias, Universidad Pedagógica y Tecnológica de Colombia UPTC, Avda. Central del Norte, Vía Paipa, Tunja, Boyacá, Colombia*

[c]*Unidad de Ingeniería Tisular, Instituto Distrital de Ciencia, Biotecnología e Innovación en salud (IDCBIS), Cra 32 #12-81, 0571 Bogotá, Colombia*

[d]*Facultad de Química, Laboratorio de Materiales Cerámicos, Universidad Nacional Autónoma de México UNAM, Avda. Universidad 3000, C.U. Coyoacán, Ciudad de México, 04510, Mexico*

[e]*Instituto de Investigaciones en Materiales, Universidad Nacional Autónoma de México UNAM, Av. Universidad, C.U. Coyoacán, 04510 Ciudad de México, Mexico*

a thermoplastic, biocompatible, and biodegradable material,[8] with a low melting temperature, although it has some disadvantages in its biomedical use, such as low osteoconductivity, low cell adhesion capacity[9] and low mechanical properties.[10]

In this sense, some research has focused on improving the properties of PLA by incorporating ceramic reinforcements, such as calcium phosphates, which are biocompatible nanocomposites and can interact or bind to living tissues.[6] In particular, β-tricalcium phosphate (TCP) is an osteoimmunomodulatory ceramic that regulates the balance between osteogenesis and osteoclastgenesis during new bone formation and is reabsorbed within 6 weeks after implantation.[11,12] PLA/TCP nanocomposites have been obtained as fibers by the electrospinning technique and as 3D scaffolds by AM.[13] Regarding the incorporation of TCP, its low resistance to fracture after sintering[14] and low toughness have been published, which limit its application as a scaffold. Based on these results, other materials such as graphene oxide nanoparticles (GONPs), have been incorporated as mechanical reinforcement.[15,16]

Graphene oxide (GO) is attached as a reinforcement is bound to the polymer matrix through the oxygenated functional groups present in its structure (epoxides, hydroxyls, carboxylic groups).[15,17,18] It has also been shown to promote osteogenesis and improve osteoconductivity when used as an interfacial phase to bond the biopolymer with bioceramics. When calcium phosphates are used, GONPs (graphene oxide nanoparticles) can absorb calcium from the phosphates due to their negative charge through electrostatic interactions.[18,19]

In this way, PLA reinforced with bioceramics such as graphene oxide/β-tricalcium phosphate (GO/TCP) is a biomaterial with high potential in the manufacture of scaffolds for the reconstruction of bone tissues. Additionally, the application of these scaffolds requires a systematic study that allows improving their bioactivity using functionalization strategies.[20]

Poly-L-lysine (POLYL) is a biocompatible cationic polymer characterized by promoting cell adhesion, proliferation and regeneration at the biomaterial interface. It has a strong affinity for proteins due to the amine groups available in lysine molecules and negative charges on the cell membrane.[21–23]

The objective of this research was to develop a scaffold for bone tissue regeneration applications comprising poly(lactic acid) reinforced with graphene oxide (GO)/β-tricalcium phosphate (TCP) bioceramics and functionalized with poly-L-lysine (POLYL). The scaffold was evaluated *in vitro* through the assessment of its capacity to support the adhesion and proliferation of hWJ-MSCs cells. Umbilical cord-derived Wharton's jelly mesenchymal stem cells (hWJ-MSCs) have a high cell yield and are readily isolated from Wharton jelly within the umbilical cord.[24] Additionally, they demonstrate superior proliferative capacity and produce more collagen than fibroblasts,[25] which is advantageous for applications in bone tissue regeneration.

Investigations have been conducted into the potential use of TCP in conjunction with carbon nanotubes, polycaprolactone (PCL),[26] and scaffolds comprising PLA, hydroxyapatite, and graphene oxide. This has been achieved through the utilization of electrospinning[27] and nanodispersion techniques.[28] However, so far there are no published reports of scaffolds combining PLA, GO, TCP, and POLYL for bone tissue engineering. The distinctive combination of materials in PLA/GO/TCP/POLYL scaffolds represents a novel approach to bone tissue engineering. Furthermore, using additive manufacturing techniques facilitates the generation of scaffolds with interconnected pores, vital for cellular infiltration and nutrient exchange.

Experimental

Materials and methods

Materials. The poly(lactic acid) (PLA) polymeric material used was supplied by NatureWorks® Ingeo™ 2003D. In turn, the reagents β-tricalcium phosphate (TCP, CAS no. 7758-87-4, purity ≥96.0%), graphene oxide (GO, reference 796034 powder, 15–20 sheets, 4–10% edge oxidized), poly(vinyl alcohol) (PVA, CAS no. 9002-89-5, molecular weight of 31 000–50 000 g mol^{-1}, 98.99% hydrolyzed), sodium hydroxide (NaOH, CAS no. 1310-73-2, ≥97.0%), were supplied by Sigma-Aldrich. The solvent dichloromethane QP was purchased from Alvi.

For cellular assays, the reagents Dulbeco's Modified Eagle Medium (DMEM, ref. 11885-084), trypLE™ express enzyme (ref. 12605-208), antibiotic antimycotic (ref. 15240-062), Bovine Serum Albumin (BSA, ref. 15260-037), Fetal Bovine Serum (FBS, ref. 16000-044) and Phosphate Buffered Saline 10× (PBS 10×, ref. 70011-044) were purchased from Gibco, Life Technologies, and Resazurin (ref. R7017) were purchased from Sigma Aldrich. Heparin (ref. 103/AP/RR/97/F/R) was purchased from Gland Pharma Ltd. Paraformaldehyde (PFA, ref. 141451) was purchased from Panreac. Phalloidin red (ref. 424203) was purchased from Biolegend. Live Dead kit (ref. L3224) was purchased from Invitrogen, and human platelet lysate (hPL) was provided from Good Manufacture Practice (GMP) group of the Instituto Distrital de Ciencia, Biotechnology e Innovación en Salud (IDCBIS) from Bogotá, Colombia.

For the surface modification of PLA, sodium hydroxide (ref. 106498), 1-ethyl-3-(3-dimethylaminopropyl) carbodiimide (EDC, ref. 03449) and *N*-hydroxysuccinimide (NHS, ref. 130672) and the poly-L-lysine (POLYL, #3438-100-01, R&D Systems, 0.1 mg mL^{-1}) were used.

Sintering of TCP and GO/TCP bioceramics. Previously, 6% w/v GO was dispersed in a 0.2 M CTAB (cetyltrimethylammonium bromide) solution for 30 minutes at 50 °C, according to the protocol previously reported by Sánchez-Cepeda *et al.*,[29] then the CTAB was removed on a Schlenk line connected to a cryogenic trap at 500 °C for 1 h, in order to obtain the GONPs. Then, the GONPs were pulverized with the TCP in a Fritsch-Germany Mini Mill Pulverisette 23 at a frequency of 15 oscillations per second for 20 minutes, until homogenization was achieved. Sintering of the TCP and GO/TCP nanocomposites was performed in a high-temperature tubular furnace, Model Lindberg Blue M Thermo Scientific at a sintering temperature of 600 °C for 1 h, using the Schlenk line and under a controlled atmosphere of argon at 20 psi. Heating rates (40 °C min^{-1}) and cooling (5 °C min^{-1}) of the furnace were employed for the sintering of the nanocomposites. These temperatures were used below the melting point of the bioceramics and, in turn, below

the phase transition temperature of α-tricalcium phosphate (1200 °C).[30,31]

Filament extrusion and FDM printing of PLA and PLA reinforced with bioceramics. The bioceramics of GO 0.1% w/w, TCP 5% w/w and GO/TCP 0.1/4.9% w/w were each dispersed in dichloromethane with ultrasound at 50 dB for 15 minutes until homogenization. Then, PLA 16% w/v was added to each solution with the bioceramics and left under magnetic stirring until dissolved. Also, a 16% w/v PLA solution was prepared as a control sample. Additionally, poly(vinyl alcohol) (PVA) 5% w/v was dissolved in distilled water at 70 °C, under stirring with ultrasound at 50 dB, and was used to form the emulsions of PLA, PLA/GO, PLA/TCP and PLA/GO/TCP, in approximately 4 to 5 minutes, Fig. 1a. The polymer composites were washed with water at 70 °C to remove PVA from the polymer matrix and dried at room temperature for 5 days.

For filament extrusion, the polymeric nanocomposites were cut into small pieces and added to the extruder chamber using Filastruder brand equipment. Right after heating the extrusion equipment to 190 °C, the polymeric nanocomposites were melted[32,33] and filaments were obtained using a circular die with a diameter of 1.75 mm, Fig. 1b.

A 3D geometric structure (cube constructed from reticular meshes) was designed using CAD (Computer Aided Design) software.[34] The scaffold was constructed using the Creality Ender-3-Pro printer, with system porosity controlled by replicating the unit cell along the x, y, and z axes, as shown in Fig. 1c. The unit cell geometry was set to a scale of 2 mm with a wall thickness of 0.05 mm. The final scaffold has a cylindrical shape, measuring 1.2 cm in diameter and 4 mm in height. The reticle rotated concerning the transverse axis of rotation every 30°.

The 3D geometric structures of the polymeric composites of PLA, PLA/GO, PLA/TCP, and PLA/GO/TCP were manufactured using additive manufacturing technology, also called Fused Deposition Modeling (FDM), where "threads" of the material used, which involved the distribution of the molten polymeric compound, layer by layer.

Characterization

FT-IR analysis. The characterization of the functional groups in the structure of the 3D polymeric nanocomposites of PLA, PLA/GO, PLA/TCP, and PLA/GO/TCP was carried out by infrared absorption spectroscopy (FT-IR), in the average infrared frequency region from 4000 to 400 cm^{-1}. Measurements were performed on a Thermo Scientific Nicolet 6700 FT-IR spectrometer, with an ATRSmart orbit attenuated total reflection (ATR) system at a resolution of 4 cm^{-1}.

X-ray diffraction (XRD). X-ray powder diffraction was used for phase characterization while monitoring the structural changes of the 3D scaffolds manufactured by FDM. The analysis was performed in a SIEMENS D-500 diffractometer, CuKα1 radiation filtered with Ni, $\lambda = 0.1542$ Å, with a time constant of 1.2 s, an angular step constant of 0.02° and a scanning range from 10° to 70° (2θ), all performed at room temperature.

Thermal properties (DSC). For thermal properties, a TA Instruments DSC Q100 differential scanning calorimeter was used, at a heating rate of 10 °C min^{-1} from an initial temperature of 10 to 260 °C min^{-1} and under a nitrogen atmosphere with a flow of 50 mL min^{-1}. From the DSC experiments, the

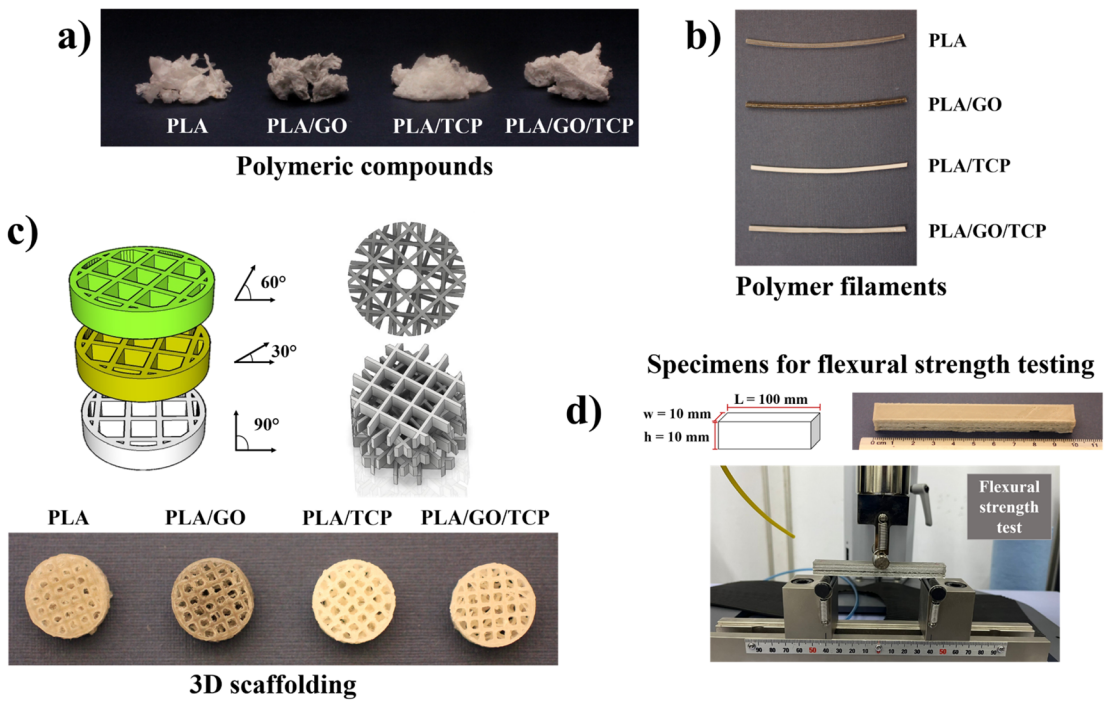

Fig. 1 PLA (16% w/v), PLA/GO (GO, 0.1% w/w), PLA/TCP (TCP, 5% w/w), PLA/GO/TCP (GO/TCP, 0.1/4.9% w/w) polymeric nanocomposites before extrusion (a); PLA and polymer filament after extrusion (b); 3D scaffolding (c) and flexural strength testing (d).

glass transition temperature (T_g), the melting temperature (T_m) and the cold crystallisation temperature (T_{cc}) were determined. The crystalline content (X_c) of PLA and the 3D polymeric nanocomposites was calculated according to eqn (1), from the difference in the enthalpy of fusion (ΔH_m) and the enthalpy of crystallisation (ΔH_c), excluding any crystallinity induced by the DSC scan itself and dividing this quantity by the enthalpy of fusion of a 100% crystalline PLA single crystal (ΔH_m, perfect crystal = 93.6 J g^{-1}):[17,35,36]

$$X_c = \frac{\Delta H_m - \Delta H_c}{\Delta H_{m,\ \text{perfect crystal}}} \quad (1)$$

Mechanical properties. The bending tests were performed in a Shimadzu AGS-X universal mechanical testing machine, according to the ASTM D790 standard at a deformation speed of 1.07 mm min^{-1}, the dimensions of the specimens were h = 10 mm (height), L = 100 mm (length) and w = 10 mm (width), Fig. 1d.

Hydrolytic degradation tests. Hydrolytic degradation tests were performed in test tubes containing 5 mL of an aqueous solution of 0.5 M NaOH (pH = 12.66) for 24 and 96 h, and the pH was measured.[37] The 3D polymeric scaffolds were then removed from the solution, the excess solution was removed and were dried at room temperature for 5 days. The samples were weighed three times, and the average weight was recorded. The swelling degree (S) was calculated using eqn (2):[38]

$$S = \frac{W_s - W_i}{W_i} \times 100 \quad (2)$$

where S is the degree of swelling, W_s is the weight of the wet sample and W_i is the weight of the initial dry sample.

Morphological analysis and surface changes on the 3D polymeric scaffolds were performed using scanning electron microscopy a JEOL JSM-7600F Field Emission type scanning electron microscope with a Schottky field-emission electron gun. Samples were coated with a thin layer of gold (Au) at 0.85 kV for 90 s using a cathode sputtering JEOL Fine Coat, Ion Sputter JFC 1100. The distribution of bioceramics TCP and GO/TCP present on the polymer matrix surface was detected using energy dispersive X-ray spectroscopy (EDS), performed on the scaffolds prior to the hydrolytic degradation tests.

Cell culture of mesenchymal stromal cells. Scaffolds PLA, PLA/GO, PLA/TCP, PLA/GO/TCP and PLA/GO/TCP/POLYL were seeded with Wharton's jelly mesenchymal stromal cells (hWJ-MSCs) or hWJ-MSCs transduced with green fluorescent protein (hWJ-MSCs-GFP). These cells (passage 4 or 5 [P4–P5] for hWJ-MSCs and passage 7 or 8 [P7–P8] for hWJ-MSCs-GFP) were cultured in DMEM supplemented with hPL, antibiotic antimycotic and heparin and maintained at 37 °C in a humid atmosphere with 5% CO_2.

Cells were seeded into T75 flasks and grown to 70–80% confluence. Cells were harvested by incubation with Tryple Express for 5 minutes at 37 °C, 5% CO_2, followed by centrifugation at 1200 rpm for 5 minutes and the pellet was resuspended in fresh culture medium. The cells were then seeded onto the scaffolds at a density of 5×10^4 cells per scaffold. The cells were left in culture for 6 h to allow for attachment and then the culture medium was completed to 500 μL.

Cell count. hWJ-MSCs-GFP on PLA, PLA/GO, PLA/TCP, and PLA/GO/TCP scaffolds were observed using Leica fluorescence microscope (LEICA DMi8-M). Photographs were taken at 24, 48, and 72 h. Using particle analysis in ImageJ software, cells on the scaffolds were counted as follows: open the image for analysis, separate the colors from the green image, adjust the image threshold, use the sharpen and find edges tools to obtain separate cells, and perform particle analysis.

Scaffold functionalization. Functionalization of PLA/GO/TCP scaffolds was performed according to the procedure proposed by Jaidev *et al.*,[39] with some modifications. Briefly, PLA/GO/TCP scaffolds were immersed in NaOH 5 M for 1 h at room temperature, then washed with deionized water to pH 7.0–7.4 and allowed to dry. Scaffolds were immersed in 6 mM solution of EDC and NHS in PBS1× for 1 h at 4 °C, after which poly-L-lysine (1 mg mL^{-1}) was added at a ratio of 1 : 3 with EDC and NHS solution and left overnight at room temperature with gentle agitation.[10] Finally, the scaffolds were removed from the reaction and allowed to dry. The functionalized scaffolds were named PLA/GO/TCP/POLYL.

X-ray photoelectron spectroscopy (XPS). Functionalization of 3D printed PLA/GO/TCP/POLYL scaffolds was analyzed using a PHI 5000 VersaProbe II equipment with a monochromatic X-ray beam source at 1486.6 eV and 15 kV. The obtained spectra were deconvoluted for analysis performed as fast detail scan of the C 1s, O 1s and N 1s regions.

Cell viability. P4–P5 cells were seeded on the scaffolds at a density of 5×10^4 cells per scaffold. Cell viability at 1, 3, 5, 7 and 14 days was analysed using a live/dead kit (Invitrogen). Briefly, a solution of 5 μL calcein and 15 μL ethidium homodimer in 15 mL PBS was prepared and added to each well. Cells were incubated for 10 minutes at 37 °C in a humid atmosphere with 5% CO_2 and visualised using a fluorescence microscopy. Digital photographs of each scaffold were taken at 10× magnification. Calcein-stained live cells were visualised using a fluorescein filter, while ethidium-stained dead cells were observed using a rhodamine filter, bright field images were also taken to visualise the scaffolds. The three images were then merged.

Cell proliferation. Cell proliferation on PLA, PLA/GO/TCP and PLA/GO/TCP/POLYL was measured by the resazurin assay (Sigma Aldrich). Briefly, hWJ-MSCs (5×10^4 cells per mL) were seeded on scaffolds as described above. After 1, 3, 5, 7 and 14 days of incubation, the cells were incubated with fresh culture medium containing 1% v/v resazurin for 3 h at 37 °C and 5% CO_2. The optical density (OD) at 570 nm and 600 nm was then measured using a spectrophotometric microplate reader (Synergy HTX, BioTek).[40]

Osteogenic differentiation. hWJ-MSCs were seeded on PLA, PLA/GO/TCP, and PLA/GO/TCP/POLYL scaffolds, and osteogenic differentiation was induced using an osteogenic medium (StemPro Osteogenesis Differentiation Kit, Life Technologies, Carlsbad, CA, USA) applied 24 hours post-seeding. The medium was replaced every three days until cells were fixed with 4%

paraformaldehyde at 7 and 14 days. Calcium deposition was then assessed using alizarin red staining (Sigma-Aldrich).

Relative expression of osteogenic genes by qRT-PCR. Total RNA from hWJ-MSCs seeded on PLA, PLA/GO/TCP, and PLA/GO/TCP/POLYL scaffolds and exposed or not to osteogenic media was isolated at 7 and 14 days post-cultured using a PureLink RNA Mini Kit (Thermo Fisher Scientific, Waltham, Massachusetts, USA) according to the manufacturer's protocol. RNA concentration and quality were evaluated in a NanoDrop-1000 instrument (Thermo Scientific NanoDrop™ 2000/2000c). All samples were normalized at 14 ng μL^{-1}. Complementary DNA was synthesized by reverse transcription of total RNA using SuperScript™ IV First-Strand cDNA Synthesis Reaction (Invitrogen, San Diego, CA, USA), followed by qRT-PCR using a 7500 Fast Real-Time PCR System (Applied Biosystems, California, USA). TaqMan probes were assessed for gene expression assays (Applied Biosystems, California, USA). Each reaction contained 5 μL of Master Mix (Applied Biosystems), 2.5 μL of molecular biology grade ultrapure water, 0.5 μL Taqman Assay and 2 μL of cDNA. Bone-specific marker genes were analyzed, including SPP1 (secreted phosphoprotein 1 or Osteopontin (OPN), Hs00959010_m1), RUNX2 (Runt-related transcription factor 2, Hs01047973_m1), BMP2 (bone morphogenetic protein 2, Hs01154192_m1), and housekeeping gen β-actin (Hs01060665_g1). To determine the PCR efficiency for each gene, the calibration curve was used based on formula $E = 10^{(-1/\text{slope})-1}$. Relative expression was subsequently calculated using the $2^{-\Delta\Delta CT}$ method, and the fold-change was normalized using housekeeping data.

Immunofluorescence. hWJ-MSCs on PLA/GO/TCP and PLA/GO/TCP/POLYL after 48 h of culture were fixed with 4% PFA, washed three times with sterile PBS, and stained with Phalloidin red (ref. 424203, Biolegend) diluted in PBS 1× at a concentration of 1 : 100. Cells were permeabilized with Triton X-100 0.5% for 10 minutes and then washed twice times with PBS 1× and BSA 0.5% and blocked with PBS-FBS 5% for 1 h at room temperature. Phalloidin red antibody was added and incubated for 10 minutes. After washing, the nuclei were counterstained with DAPI at a final concentration of 0.1 μg mL^{-1} for 5 minutes. Imaging was performed using a Confocal microscope (Olympus Fv1000).

Results and discussions

FTIR characterization

The FT-IR spectrum of PLA and 3D polymeric scaffolds with GO, TCP and GO/TCP sintered at 600 °C for 1 h are observed in Fig. 2a. The uniform dispersion of reinforcement such as TCP and GO/TCP in the polymer matrix usually improves the interactions between the load and the matrix. The spectrum of PLA pellets is used as a reference for 3D polymeric nanocomposites. Its absorption bands are characteristic of the lactic acid ester group and are observed at 1747 cm^{-1} and 1179 cm^{-1} for –C═O– and –COC–, respectively. It presents asymmetric stretching vibrations of the $-CH_3$ group at 2997 cm^{-1} and symmetric C–H vibrations at 2947 cm^{-1}. The bands corresponding to the CH_3 bending vibrations were found at 1455 cm^{-1} and the C–O–O stretching vibration at 1080 cm^{-1}.[41]

For the 3D polymeric scaffolds with TCP and GO/TCP, Fig. 2b and c, respectively, the PO_4^{3-} groups show characteristics of the β phase, associated with a tetrahedral apatite structure with asymmetric and symmetric deformation bands of the group $[PO_4]v_4$ (O–P–O) at 579 and 617 cm^{-1} for TCP and a triple band for GO/TCP at 567, 586 and 618 cm^{-1}, in addition, the bands of the group $[PO_4]v_2$ (O–P–O) with bending variations for the TCP are observed at 535 and 551 cm^{-1} and for the GO/TCP at 539 and 549 cm^{-1}. The absorption bands that correspond to a symmetric stretching mode $[PO_4]v_1$ for TCP are observed at 968 cm^{-1} and for GO/TCP at 979 cm^{-1}.[42] The C–H stretching vibrations for methyl ($-CH_3$) and methylene (–CH) confirm that they are organic based and contain at least one aliphatic fragment or center. Also, it is observed that the 3D polymeric scaffold with GO and GO/TCP present a band that corresponds to the C–C vibration at approximately 1514 and 1515 cm^{-1}, respectively.[41]

The above results confirm that bioceramics are incorporated as reinforcements in the PLA polymer matrix and their uniform dispersion improves the interactions between the filler and the matrix.

Crystallinity by XRD

In Fig. 2d, it is observed that the PLA and PLA/GO 3D polymeric scaffolds are mainly amorphous due to the second extrusion when the material is printed by FDM, similar to what was reported by Backes *et al.*,[13] in this process, the molten PLA material cools quickly to take it to 3D printing, affecting its crystalline structure,[17] unlike the characteristic reflection signal of PLA pellet at 16.5° 2θ according to JCPDS 00-054-1917.[43]

PLA nanocomposites reinforced with TCP have a crystallinity index of 31%, showing characteristic diffraction signals of β-tricalcium phosphate at 27.83°, 31.07°, 34.41° 2θ assigned to (2 1 4), (0 2 10), (2 2 0) planes, respectively.

The nanocomposites reinforced with GO/TCP showed a crystallinity index of 32%, with diffraction signals at 27.81°,31.03°, 34.39° 2θ assigned to the planes (2 1 4), (0 2 10), (2 2 0), respectively, according to JCPDS TCP (055-0898) and GO (041-1487).[29,44]

The characteristic diffraction signals of GO (26.4° y 42.2°) overlap with those of TCP due to the low content and good dispersion in the polymer matrix.[41] These results allow us to observe changes due to the thermal processes of the polymer and, in turn, confirm of the incorporation of ceramics.[18]

Thermal properties and crystallinity content

In Fig. 3a, the DSC thermograms of the 3D polymeric scaffolds shows an endothermic signal associated with the glass transition temperature (T_g) is observed, an exothermic transition that corresponds to the cold crystallization temperature (T_{cc}) and an endothermic change where fusion occurs (T_m). The results of these analyses, and the crystalline content (X_c), calculated from eqn (1), are summarized in Table 1. The T_g of the scaffolds

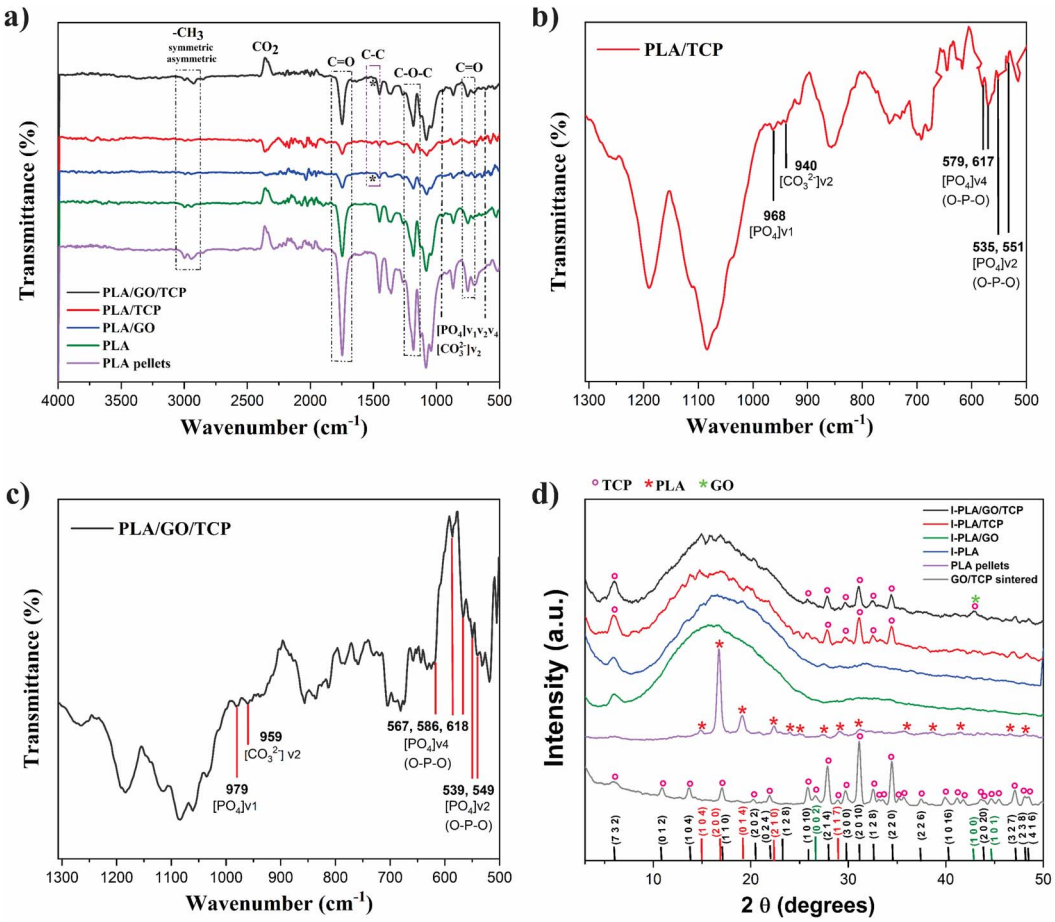

Fig. 2 FTIR spectra for PLA pellets and 3D scaffolds PLA, PLA/GO, PLA/TCP and PLA/GO/TCP (a), TCP characteristic bands are evident in PLA/TCP (b) and PLA/GO/TCP (c); XRD of GO/TCP sintered for one hour, PLA pellets and PLA, PLA/GO, PLA/TCP and PLA/GO/TCP 3D scaffolds (d).

increases slightly with respect to T_g of PLA, at 1.6% with GO, 2.7% with TCP, and 3% with GO/TCP, the composites become brittle, hard, and behave similarly to a ceramic glass.

For its part, the percentage of crystallinity (% X_c) is affected by the presence of bioceramics and increases due to TCP, increasing its value up to 2.8 times with respect to PLA. This result is similar to those observed by Siqueria *et al.*[45] However, it has the opposite effect with GO, it decreases its % X_c by 4%, which shows that scaffolds with GO is meanly amorphous.

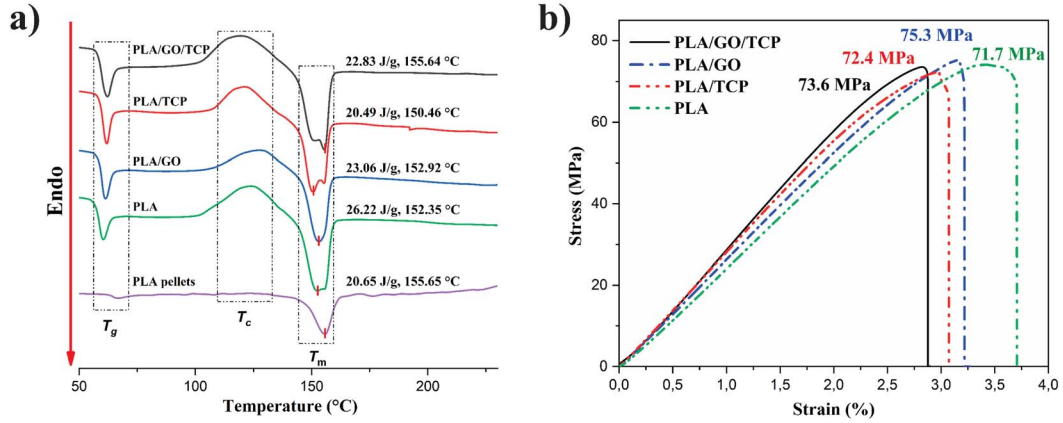

Fig. 3 Differential scanning calorimetry (DSC) of PLA pellets and PLA, PLA/GO, PLA/TCP and PLA/GO/TCP 3D scaffolds (a); Flexure–strain curves corresponding to PLA, PLA/GO, PLA/TCP and PLA/GO/TCP 3D scaffolds (b).

Table 1 Thermal results of 3D polymeric composites

Samples	T_g (°C)	ΔH_g (J g^{-1})	T_{cc} (°C)	ΔH_c (J g^{-1})	T_m (°C)	ΔH_m (J g^{-1})	X_c (%)
PLA pellets	66.64	1.138	—	—	155.65	20.65	—
PLA scaffold 3D	60.01	4.866	123.94	24.64	152.35	26.22	1.69
PLA/GO scaffold 3D	60.98	5.508	128.28	18.97	152.92	20.49	1.62
PLA/TCP scaffold 3D	61.63	5.063	121.98	18.58	150.46	23.06	4.79
PLA/GO/TCP scaffold 3D	61.81	5.005	120.39	25.82	155.64	22.83	3.19

Additionally, the increase in the percentage of crystallinity is associated with the fusion process. In the cold crystallization stage, the same happens in the PLA 3D scaffold.

For the T_{cc} of the 3D polymeric scaffolds with GO increased, suggesting that GO provides heterogeneous nucleation sites to improve the cold crystallization ability, the mobility of PLA chains, and exerts dual effects on the crystallization behavior.[46,47]

The ΔH_c values with GO/TCP nanocomposites increased significantly, affecting the crystallization of the scaffolds and less degradation due to a decrease in melt viscosity and the reduction of the polymer chain length at higher temperatures, generating greater chain mobility.[47]

For the T_m of the compounds, it decreases relatively, but it is very close to the theoretical value of PLA (T_m 155.65 °C and ΔH_m 20.65 J g^{-1}), the addition of inorganic particles such as TCP (5% w/w) and GO/TCP (0.1/4.9% w/w), does not modify the melting temperature of PLA, but does contribute to the appearance of double fusion signals that are originated from the fusion-recrystallization mechanism or from the presence of crystals with different crystalline forms or different degrees of perfection,[46] polymorphism, where T_{m_1} corresponds to the fusion of spherulites (formed at a lower crystallization temperature) and T_{m_2} corresponds to the fusion of hexagonal crystals (formed at a higher crystallization temperature high and the most stable α form).[36,48]

Mechanical testing

Fig. 3b and Table 2, show the results of the bending tests of the 3D polymeric scaffolds where a decrease in the elastic modulus of the PLA/GO and PLA/TCP 3D polymeric scaffolds were observed, unlike the scaffolds with GO/TCP nanocomposites that present a higher elastic modulus improved by the reinforcing nanomaterials.

The maximum resistance follows the trend: PLA/GO > PLA/GO/TCP > PLA/TCP > PLA. The behavior of the scaffold PLA/GO/TCP may be attributed to the second extrusion that the 3D polymer scaffolds present and the properties of the reinforcing nanocomposites that make a thermal barrier during the second extrusion to prevent degradation of the polymer. Such a situation takes place because the nanocomposites dispersed in the polymer matrix cause a strong interfacial adhesion between the GONPs and the PLA matrix, reducing the mobility of the PLA chains in the vicinity of the surface of the GONPs, leading to great stability of the polymer matrix.[46] PLA in pellets without any heat treatment has an elastic modulus of 3.5 GPa,[49] proving that when the polymer is subjected to heat treatments, it undergoes degradation.[50] The Young's modulus values of 2.6–2.9 GPa, determined by bending tests for the PLA-TCP-GO composites, are within the range reported for trabecular bone (cancellous), which exhibits high porosity and presents moduli between 1.1 and 15 GPa.[51] This range depends on the specific architecture and intrinsic material properties of trabecular bone indicating potential suitability for applications that require materials compatible with this type of bone structure.

Table 2 Young's modulus, standard deviation and maximum resistance of 3D polymeric nanocomposites

Samples scaffolds 3D	Young's modulus (MPa)	Standard deviation (MPa)	Maximum resistance (MPa)
PLA	2602.6	286.1	71.7
PLA/GO	2417.2	290.3	75.3
PLA/TCP	2361.8	517.4	72.4
PLA/GO/TCP	2958.3	16.3	73.6

Morphologic characterization

The EDS spectra of the surface of the 3D scaffolds before the degradation tests are shown in Fig. 4. In the spectrum of the PLA 3D scaffold, Fig. 4a, C (59.83%) and O (39.86%) signals are observed, which is characteristic of the polymer chemical composition. The elemental composition of the PLA/GO 3D scaffold, Fig. 4b, revealed the presence of carbon (53.58%) and a higher percentage of oxygen (45.75%), characteristic of the presence of the graphene oxide in the polymer matrix.[52]

The 3D PLA/TCP scaffold, shown in Fig. 4c, exhibited an elemental composition of carbon (60.09%) and oxygen (37.27%). Additionally, calcium (1.57%) and phosphorus (1.07%), characteristic elements of the tricalcium phosphate.[53]

The spectrum of the 3D PLA/GO/TCP scaffold, shown in Fig. 4d, displayed the elemental distribution within the polymeric matrix, verifying the incorporation of GO and TCP bioceramics.[54,55] The Au present in the 3D scaffolds is the result of the coating of the scaffolds for SEM observations.

In Fig. 5, the morphology of the 3D polymeric scaffolds is observed after the swelling and biodegradability tests at 24 h and 96 h in an aqueous medium of 0.5 M NaOH and these results are summarized in Table 3. For the 3D PLA polymeric scaffold, the surface of the scaffold at 24 h is observed to be flat with some shallow surface characteristics (grooves, wells and notches), its initial weight without treatment was 0.257 g and after the test it was 0.162 g with a swelling percentage of 0.13%. At 96 h, the scaffold pore looks wide and has a surface with indentations and wells. Its initial weight was 0.261 g and after

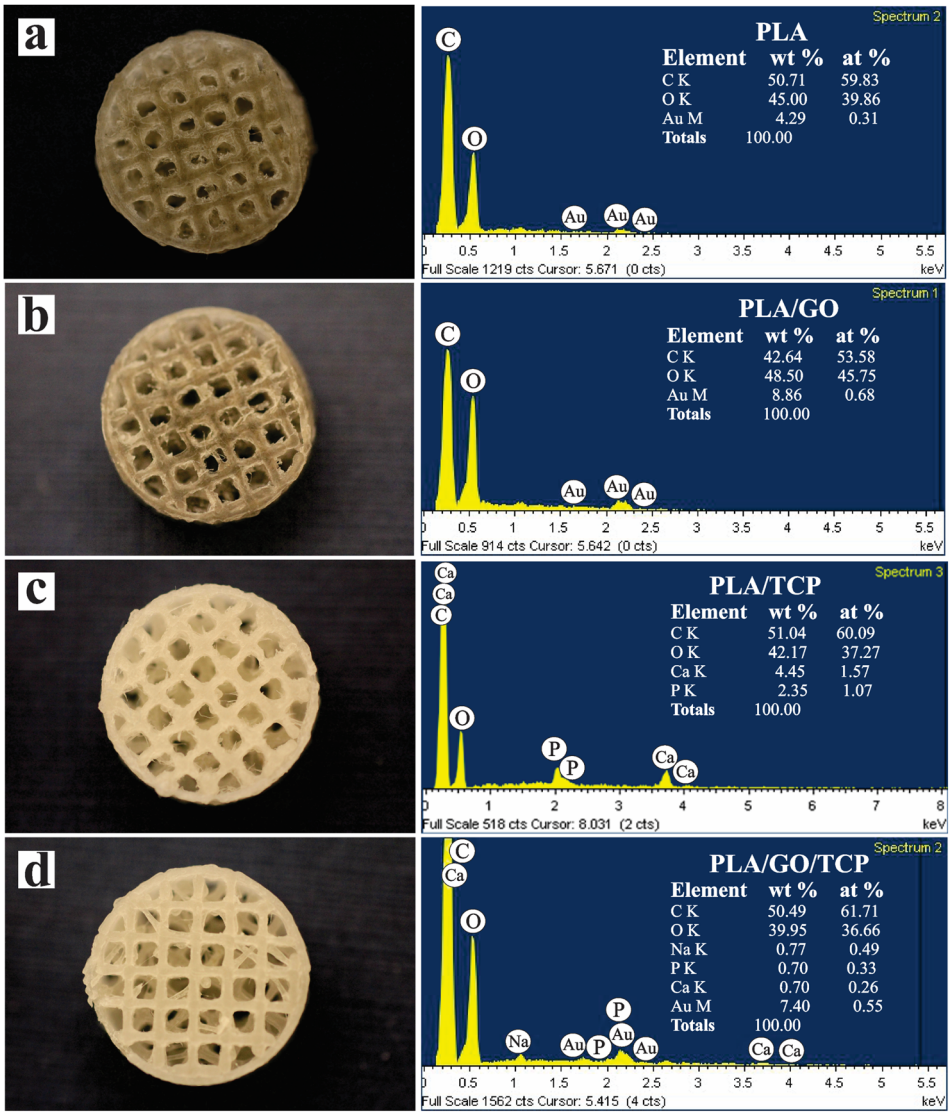

Fig. 4 Photographic image and energy dispersive X-ray (EDS) spectra of the surface of 3D scaffolds PLA (a), PLA/GO (b), PLA/TCP (c) and PLA/GO/TCP (d).

the test it was 0.211 g with a swelling percentage of 60.76%. The polymer matrix undergoes structural changes where surface hydrolysis is caused by increased cleavage of ester bonds as more OH groups are introduced into PLA.[56]

For the 3D PLA/GO polymeric scaffold with GONPs dispersed throughout the matrix, it maintains a smooth surface with grooves and wells. Its initial weight without treatment was 0.203 g and after the test it was 0.181 g with a swelling percentage of 88.36%. At 96 h, the surface appears rough with deeper grooves and pits. Its initial weight without treatment was 0.237 g and after the test it was 0.192 g with a swelling percentage of 64.98%.

For the 3D polymer scaffolds with TCP and GO/TCP, a considerable loss of polymer matrix is observed, increasing the surface roughness and exposing the nanocomposites as the degradation time progresses. Also, it is observed that the homogeneous dispersion of bioceramics in dichloromethane with ultrasound when the nanocomposites are formed, maintains a spatial distribution of these when deposited layer by layer during printing.

For the 3D PLA/TCP polymeric scaffold, at 24 h its initial weight without treatment was 0.246 g and after the test, it was 0.197 g with a swelling percentage of 59.54%. At 96 h, its initial weight without treatment was 0.249 g and after the test it was 0.153 g with a welling percentage of 45.05%.

The TCP nanocomposites have an irregular morphology with a grain diameter of 3.59 μm. For the 3D PLA/GO/TCP polymeric scaffold, at 24 h, its initial weight without treatment was 0.280 g, and after the test, it was 0.243 g with a swelling percentage of 46.37%.

At 96 h, its initial weight without treatment was 0.232 g and after the test it was 0.120 g with a swelling percentage of 53.45%. The GO/TCP nanocomposites present an irregular morphology with a grain diameter of 4.73 μm.

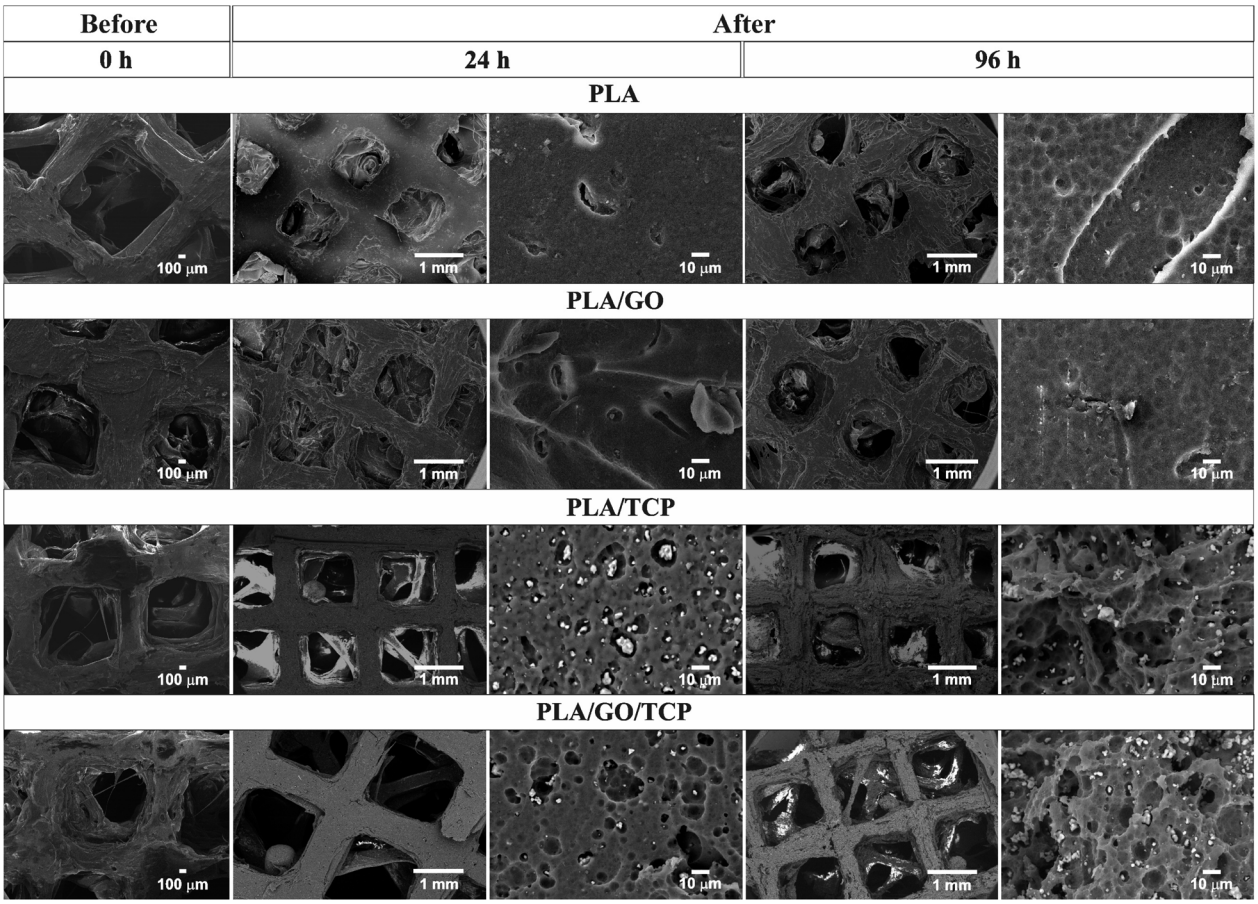

Fig. 5 SEM of three-dimensional PLA, PLA/GO, PLA/TCP and PLA/GO/TCP 3D scaffolds after degradation treatment with 0.5 M NaOH for 24 and 96 h.

Table 3 Data from degradation tests of 3D scaffolds[a]

Samples scaffolds 3D	Time (h)	$W_iS = 0$ min (g)	W (g)	pH	S (%)	Mass loss (%)	Time (h)	$W_iS = 0$ min (g)	W (g)	pH	S (%)	Mass loss (%)
PLA	**24**	0.257	0.162	12.79	0.13	36.96	**96**	0.261	0.211	12.81	60.76	19.15
PLA/GO		0.203	0.181	12.88	88.36	10.83		0.237	0.192	12.81	64.98	18.98
PLA/TCP		0.246	0.197	12.69	59.54	19.91		0.249	0.153	12.18	45.05	38.55
PLA/GO/TCP		0.280	0.243	12.76	46.37	13.21		0.232	0.120	12.49	53.45	48.27

[a] S is the degree of swelling, W is the weight of the wet sample, W_iS is the weight of the initial dry sample.

The degradation of PLA under alkaline conditions was the result of hydrolysis. The attack occurs from the hydroxide anion to the carbonyl carbon of the ester group, which generates a tetrahedral intermediate. The hydroxyl attached to the tetrahedral intermediate can leave, resulting in the generation of the ester. However, the ether connected to the tetrahedral intermediate (RO–) can also leave, resulting in hydrolysis; in other words, the generation of an alcohol group and a carboxylic acid, as shown in Fig. 6.[57] Introducing OH groups to the PLA surface would improve the surface roughness and cell affinity compared to smooth surfaces.[56] The micrographs indicate that the scaffolds maintain internal porosity and pore interconnection to provide diffusion of the aqueous medium inside the polymer matrix. Pore interconnectivity is an essential characteristic for tissue regeneration, in which it facilitates nutrient perfusion and increases cell migration, as described by Jaidev *et al.*[39]

Cell adhesion

After 24 h of culture, none of the cells in the scaffolds have the characteristic fibroblast-like morphology. Only in the PLA/GO/TCP shows this morphology after 48 h of culture, Fig. 7a. On the other scaffolds, the morphology is rounded in almost all cells at 48 and 72 h. From the cell count graph, Fig. 7b, it can be seen that at 72 h, PLA/GO/TCP is the scaffold that presents the most adhere cells. In this study, we observed that GO does not

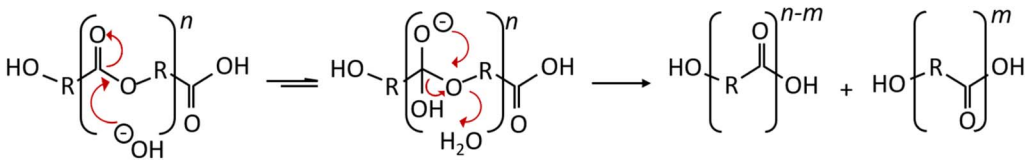

Fig. 6 Hydrolysis catalyzed by an alkaline catalyst of polyester.

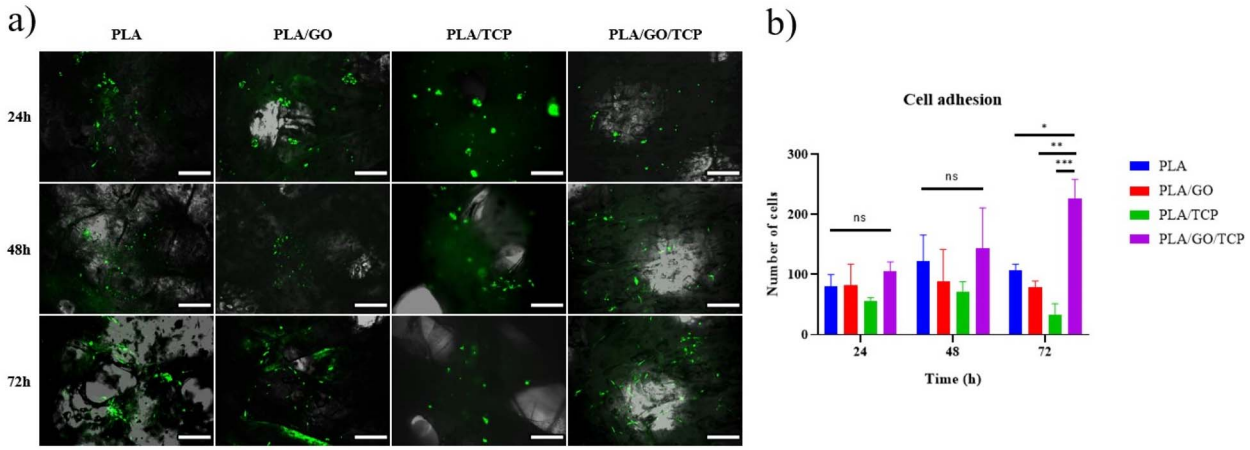

Fig. 7 Cell adhesion images (a) and cell adhesion count (b) at 24, 48 and 72 h of hWJ-MSCs-GFP seeded on PLA, PLA/GO, PLA/TCP, and PLA/GO/TCP. Scale bar 500 μm. * = $p \leq 0.05$, ** = $p \leq 0.01$, *** = $p \leq 0.001$, **** = $p \leq 0.0001$.

improve cell adhesion. Nonetheless, its incorporation mainly improves mechanical properties and the coupling agents between the polymer matrix and the ceramic.[58,59]

On the other hand, TCP has been reported as an enhancer of biological properties combined with PLA, improving cell adhesion of Mouse embryo osteoblast precursor cells (MC3T3-E1).[60] Also, encapsulated in gelatin/sodium alginate hydrogels, enhancing adhesion of bone marrow mesenchymal cells.[38]

However, we found that TCP in PLA matrix did not increase cell adhesion of hWJ-MSCs-GFP. Instead, we found that GO combined with TCP in a PLA matrix, increased cell adhesion of hWJ-MSCs-GFP up to 72 h of culture, mainly because this combination allows GO to couple TCP and PLA;[59] therefore increasing the availability of the scaffold PLA/GO/TCP for cell adhesion. These findings suggests that the synergistic.

Functionalization and X-ray photoelectron spectroscopy (XPS) analysis

Since the PLA/GO/TCP scaffold showed the highest hWJ-MSCs-GFP adhesion (Fig. 7), for this reason, we wanted to improve the biological properties of this scaffold by functionalization using carbodiimide chemistry[39] and POLYL which enhances cell adhesion on different surfaces due to its strong interaction with cell membranes.[61]

Furthermore, the chemical and morphological changes of the polymer surface caused by the negative charges of the carboxylic groups generated during the nucleophilic attack of hydrolysis,[37,62] and the coupling of the carbodiimide,[39] did not alter the integrity of the 3D printed PLA.

The spectra obtained by XPS were compiled to demonstrate the unfunctionalized and functionalized PLA surface with POLYL chemistry. In Fig. 8a, the spectrum of the PLA/GO/TCP scaffold was observed, where the main photoelectron peaks for C1s and O1s show the typical binding species of PLA.[63] The deconvoluted spectra of C1s describe different chemical states: C–C/C–H (281.62 eV), C–O (283.34 eV) and O=C–O (286.11 eV).

The deconvolved spectra of O1s describe the chemical states of O=C (529.13 eV), and O–C (530.74 eV). For the 3D PLA/GO/TCP/POLYL scaffold, Fig. 8b, the deconvolved spectra of C1s were observed where the binding energies are found in C–C/C–H (281.69 eV), C–O (283.64 eV) and O=C–O (285.88 eV), in addition, a peak at 1222 eV was observed by the treatment with POLYL.[16]

The results showed a decrease in the band intensities due to be the availability of C atoms in each functional state. The O1s spectra shows two peaks for O=C and O–C at 529.11 and 530.74 eV, respectively, in addition to a peak at 975 eV. The N1s showed that the NH_2 peak is observed at 195 and 396.61 eV and where it was attributed to the nitrogen of the amine groups of the POLYL chains.

Cell viability and proliferation

We compared the functionalized scaffold (PLA/GO/TCP/POLYL) with PLA and PLA/GO/TCP regarding hWJ-MSCs viability and proliferation. For all scaffolds, cell numbers were increased between days 3 and 5, though the cells did not yet exhibit the characteristic fibroblast-like morphology of hWJ-MSCs. This morphology began to develop on the PLA/GO/TCP/POLYL

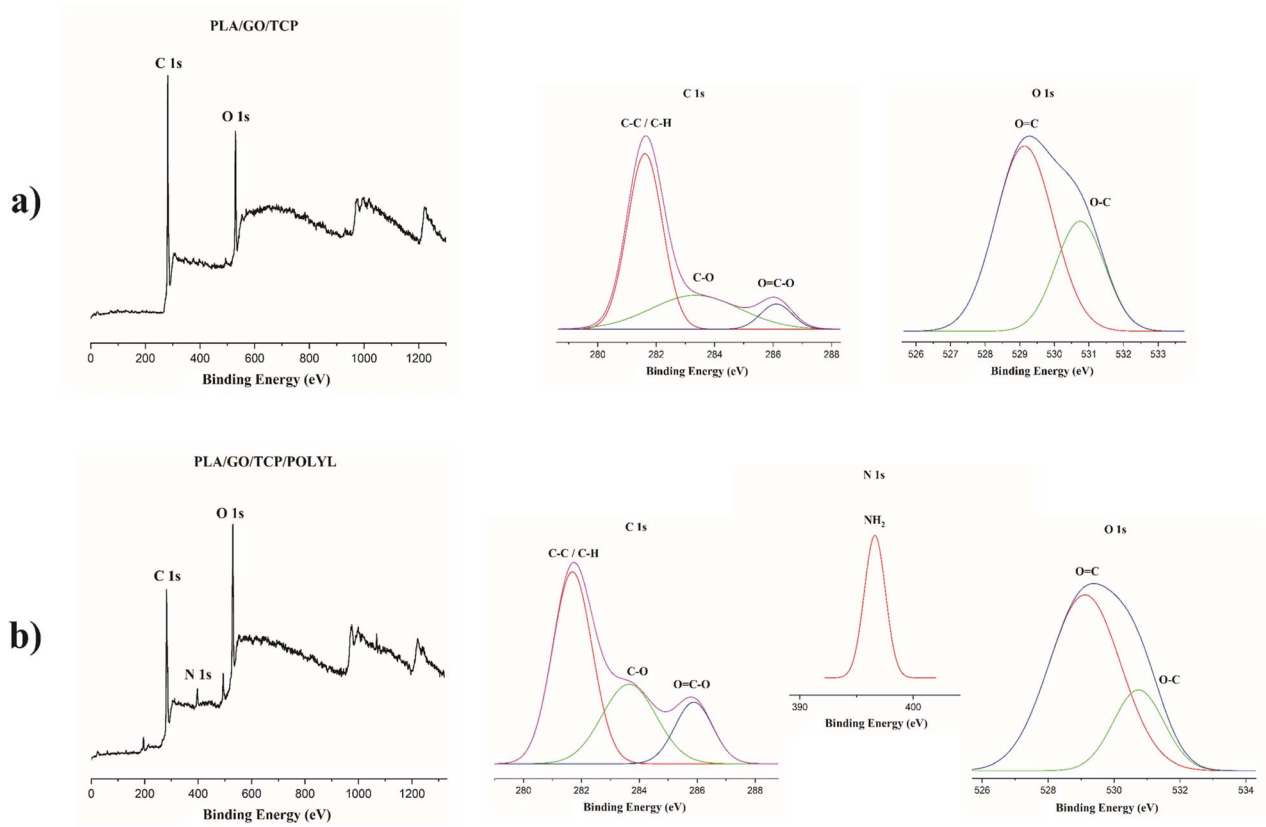

Fig. 8 XPS spectra of PLA/GO/TCP 3D scaffold for the elements C, O and N, untreated (a) and surface modified by POLYL (b).

scaffold by day 5, where the cells also appeared to occupy a larger surface area than those on PLA and PLA/GO/TCP. Dead cells were detected as early as day 1 on PLA/GO/TCP, day 3 on PLA, and day 5 on PLA/GO/TCP/POLYL, Fig. 9a. Likewise, a resazurin assay was performed to evaluate the proliferation of hWJ-MSCs on the scaffolds, Fig. 9b. This assay showed that the PLA/GO/TCP scaffold displayed the highest proliferation rate up to day 3. However, from day 5, hWJ-MSCs on the PLA/GO/TCP/POLYL scaffold showed a marked increase in proliferation by day 14, around 140%, Fig. 9b.

Including POLYL within the PLA/GO/TCP matrix notably enhanced cell viability and proliferation and facilitated the transition to a fibroblast-like morphology. The early appearance of this morphology and increased cell spreading on PLA/GO/TCP/POLYL suggest improved cell adhesion and distribution, consistent with prior studies indicating that POLYL enhances cell–material interactions and promotes proliferation.[21]

Notably, proliferation rates on PLA/GO/TCP/POLYL increased significantly after day 5, indicating that POLYL provides a favourable microenvironment for cell growth and division. The enhanced performance of PLA/GO/TCP/POLYL can also be attributed to the incorporation of GO, as evidenced by previous studies,[64–66] which can provide structural defects and surface charge[67] that promote cell adhesion and proliferation by creating a rougher surface with more sites for cell attachment.[68,69]

Osteogenic differentiation

The osteogenic differentiation assay showed significant differences in the potential of the scaffolds to promote osteogenic differentiation. The PLA/GO/TCP/POLYL scaffold was the one that promoted the highest osteogenic differentiation of hWJ-MSCs compared to PLA and PLA/GO/TCP, Fig. 10. Notably, the hWJ-MSCs on PLA/GO/TCP/POLYL scaffold produced high calcium deposits at 7 and 14 days, regardless of the culture medium (DMEM or osteogenic), indicating that the scaffold can induce osteogenic differentiation of hWJ-MSCs. In contrast, PLA and PLA/GO/TCP scaffolds showed no mineralization at 7 days in DMEM and minimal mineralization at 14 days, even lower than their mineralization at 7 days in osteogenic medium, Fig. 10a.

The incorporation of GO into the scaffold significantly enhanced the osteogenic differentiation of hWJ-MSCs, as evidenced by increased staining of calcium deposition by alizarin red,[70,71] the synergistic effect of GO, TCP and POLYL along with PLA can be attributed to the ability of TCP to provide a structural support for cell growth and mineralization,[72] while GO and POLYL enhance cellular interactions and signaling pathways.[73]

Previous studies have demonstrated that the incorporation of GO, TCP, and POLYL into biomaterials can enhance cell adhesion, proliferation, and differentiation. For instance, GO has been shown to improve cell adhesion and proliferation by providing a suitable surface for cell attachment.[74] Similarly, TCP

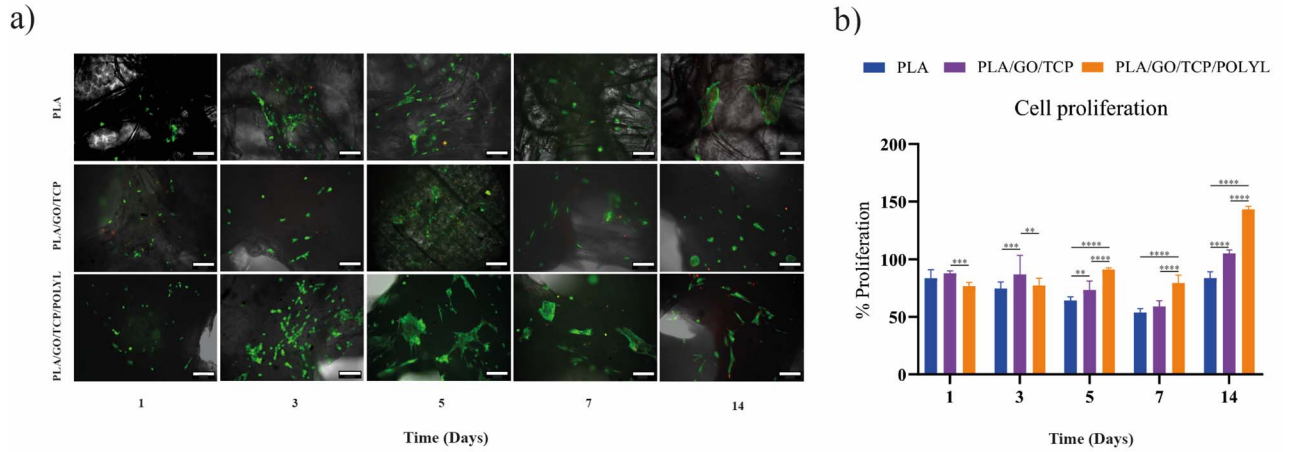

Fig. 9 Viability images (a) and cell proliferation by resazurin assay (b) at 1, 3, 5, 7 and 14 days of hWJ-MSCs on PLA, PLA/GO/TCP and PCL/GO/TCP/POLYL. Scale bar 100 μm, * = $p \leq 0.05$, ** = $p \leq 0.01$, *** = $p \leq 0.001$, **** = $p \leq 0.0001$.

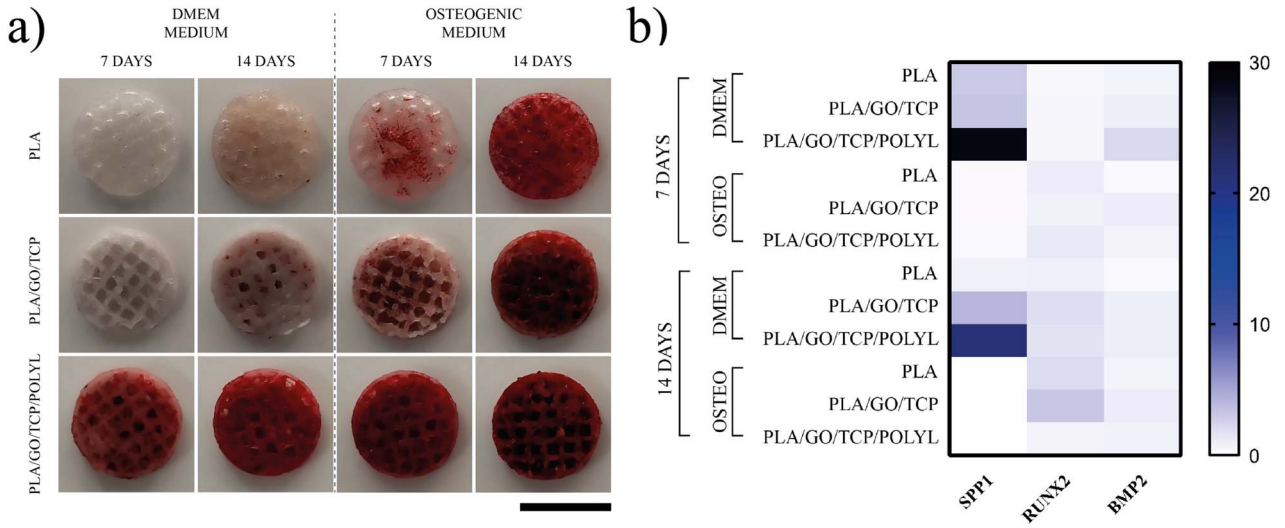

Fig. 10 The mineralization of the scaffolds was observed through Alizarin Red S staining. PLA, PLA/GO/TCP, and PLA/GO/TCO/POLYL scaffolds were seeded with hWJ-MSCs and cultured in a supplemented DMEM medium and an osteogenic differentiation medium. After 7 and 14, these were stained. Scale bar in black, bottom right = 1 cm (a). Illustrates the gene expression of SPP1, RUNX2, and BMP2 of hWJ-MSCs seeded on PLA, PLA/GO/TCP, and PLA/GO/TCO/POLYL with supplemented DMEM medium and osteogenic differentiation medium at 7 and 14 days (b).

can release calcium ions, stimulating osteogenic differentiation.[75] POLYL, on the other hand, can promote cell adhesion and proliferation through electrostatic interactions.[22]

Our findings corroborate these previous studies, as we observed that the combination of GO, TCP, and POLYL in our scaffold significantly promoted cell viability, proliferation, and osteogenic differentiation, leading to accelerated and enhanced mineralization.

Functionalized 3D scaffolds promote gene expression involved in hWJ-MSCs osteogenic differentiation

Osteopontin (OPN or SPP1), RUNX2, and BMP2 are crucial regulators of osteogenic differentiation, and an array of biomaterials can influence their expression. BMP-2 is a member of the TGF-β superfamily of growth factors earliest expressed in osteogenesis, acting as a trigger for differentiation. Once BMP2 binds to its receptors on mesenchymal stem cells (MSCs) or pre-osteoblasts, it activates downstream signaling pathways, particularly the Smad1/5/8 pathway, which initiates the expression of key transcription factors like RUNX2.[76] In this study, we reported a notable expression of BMP2 only in hWJ-MSCs seeded on PLA/GO/TCP/POLYL scaffolds in the absence of an osteogenic growth medium at 7 days post-culture, with a twofold increase in expression (Fig. 10b).

Likewise, RUNX2 expression levels were increased in hWJ-MSCs seeded on PLA and PLA/GO/TCP scaffolds cultured in the osteogenic medium after 14 days. Specifically, RUNX2 expression increased twofold in the PLA group and threefold in the PLA/GO/TCP group (Fig. 10b). RUNX2 is a key regulator of

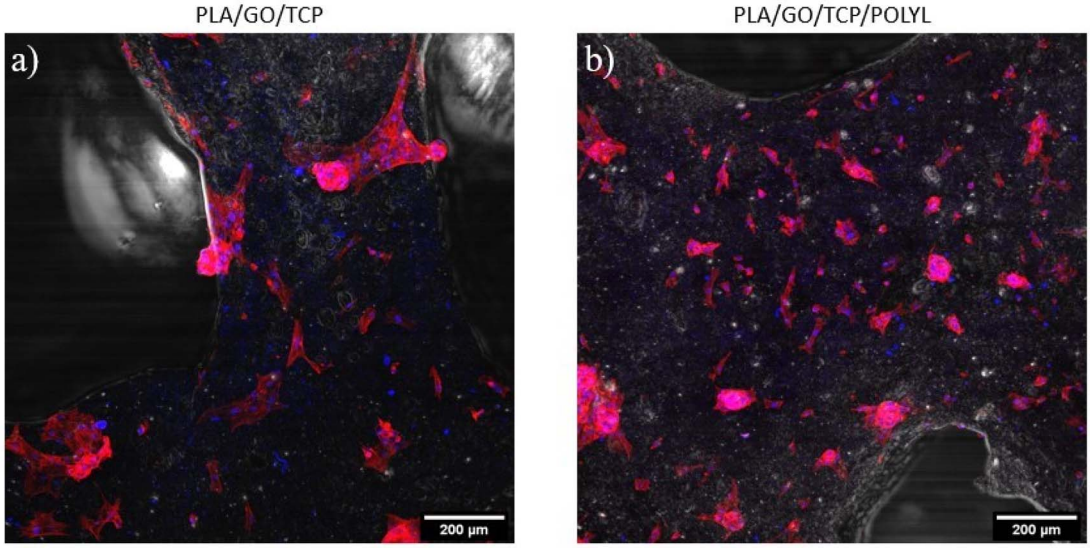

Fig. 11 Confocal microscopy images of hWJ-MSCs seeded on PLA/GO/TCP (a) and PLA/GO/TCP/POLYL (b) at 48 h.

osteoblast differentiation and bone formation. This factor initiates osteoblast differentiation by regulating the expression of essential genes involved in bone matrix production, including collagen type I (COL1) and alkaline phosphatase (ALP). Also, it regulates the process of mineralization, including the production of hydroxyapatite, and directly controls the expression of other transcription factors and genes related to bone formation, including osteocalcin (OCN) and osteopontin (OPN).[77]

OPN was expressed in high levels by hWJ-MSCs seeded on PLA/GO/TCP/POLYL scaffolds (28-fold increase at 7 days and a 21-fold increase at 14 days). These results with increased BMP2 expression showed that these scaffolds can promote osteogenic differentiation in the absence of an osteogenic differentiation medium (Fig. 10b). OPN has been demonstrated to promote osteoblast differentiation and mineralization, while also enhancing cell adhesion. This enables interaction between osteoblasts and osteoclasts with the extracellular matrix (ECM).

Although there was no significant increase in RUNX2 expression in this study, BMP2 may have prompted the rise in OPN levels. This growth factor has been demonstrated to trigger several signaling pathways, including Wnt/β-catenin, MAPK, PI3K/Akt, and Notch, extending beyond RUNX2. These pathways act in concert to drive the differentiation of mesenchymal stem cells or progenitor cells into mature osteoblasts, regulating matrix production and enhancing mineralization.[78]

On the other hand, GO can induce osteogenic differentiation by promoting key transcription factors such as RUNX2 and OPN. It enhances the proliferation and mineralization of osteoblasts, which is crucial for bone tissue formation. It acts through mechanical stiffness, surface chemistry, and biochemical cues, modulating the PI3K/AKT, MAPK, and Wnt signaling pathways, all involved in osteogenesis and cellular responses to GO.[65,79,80]

The upregulation of osteogenic markers such as OPN and BMP2 in hWJ-MSCs seeded on functionalized scaffolds containing GO in the absence of osteogenic differentiation-inducing mediators (medium of osteogenic growth) might also be related to combining the materials and 3D structure of scaffolds that promote the migration of nutrients and waste in scaffolds and infiltration and communication between cells.[81,82]

Immunofluorescence

The cytoskeleton and nuclei of hWJ-MSCs was evaluated by immunofluorescence in a confocal microscope, evidencing cell adhesion to the surface of the PLA/GO/TCP and PLA/GO/TCP/POLYL scaffolds, Fig. 11.

It was evident that the cells distribution through the PLA/GO/TCP/POLYL scaffold was better, and the hWJ-MSCs had obtain its characteristic fibroblast-like morphology. F-actin staining allows to demonstrate the morphology and distribution of hWJ-MSCs seeded on the scaffolds.

Conclusions

The development of 3D printed PLA scaffolds modified with bioceramics such as calcium phosphates, CaP, and GO nano reinforcements has been a strategy in tissue engineering to promote osteogenesis. The incorporation of GO/TCP nanocomposites in the polymer matrix increased the elastic modulus of the scaffolds. In addition, it created a thermal barrier during extrusion, preventing degradation of the polymer during AM manufacturing. 3D printing of these polymeric nanocomposites was successfully obtained while maintaining a controlled morphology and pore interconnection. The functionalization of PLA/GO/TCP scaffolds with POLYL significantly enhanced the viability, proliferation, and osteogenic differentiation of hWJ-MSCs. These cells exhibited an early fibroblast-like morphology when seeded on PLA/GO/TCP/POLYL and presented high proliferation rates up to 140%. Additionally, the

scaffolds significantly promoted osteogenic differentiation and calcium deposition at both 7 and 14 days, confirmed by alizarin red staining, even in the absence of osteogenic growth factors. This was further supported by the upregulation of key osteogenic markers, BMP2 and SPP1. Given its favorable physicochemical, mechanical, and biological properties, the PLA/GO/TCP scaffold functionalized with POLYL *via* carbodiimide chemistry holds significant potential for the repair of bone defects.

Data availability

The data supporting the findings of this study were collected during the completion of a doctoral dissertation and are currently stored on a personal computer. Due to data protection, they are not available in a public repository. However, the data may be accessed upon reasonable request. Contact Angela Patricia Sanchez Cepeda *via* email to angelapatricia.sanchez@uptc.edu.co.

Author contributions

All authors contributed to the investigation, methodology, writing – original draft, writing – review, formal analysis & editing.

Conflicts of interest

The authors have no conflicts of interest to declare with respect to the research, authorship and publication of this article.

Acknowledgements

This work was supported by MINCIENCIAS Acuerdo 757–2016 and Pedagogical and Technological University-UPTC in Colombia, CONHACYT Project CF-19 140617, UNAM Project PAPPIT IG200423 and Materials Research Institute, in México, and Unidad de Ingeniería Tisular, Instituto Distrital de Ciencia, Biotecnología e Innovación en salud IDCBIS in Colombia. This work is dedicated to the memory of our colleague Efrén de Jesús Muñoz Prieto, who passed away in 2019 and provided valuable ideas. The authors thank the collaboration of the Materials Research Institute of the National Autonomous University of Mexico, PhD Alfredo Maciel, PhD Filiberto Figueroa, Ing. Sebastián Fragoso, MsC Erick Robles and the academic technicians Miguel Canseco, Adriana Tejeda, Eliezer Hernández, Karla Reyes, Lázaro Huertas, Gerardo Cedillo, Carlos Flores, Carlos Ramos and Omar Novelo, Josué Romero, Lourdes Bazán (LUME) for technical assistance. PhD Ricardo Ballinas and PhD Cecilio Álvarez from the Institute of Chemistry. Q. Ana Reyes from the Ceramics Laboratory of the Faculty of Chemistry. PhD Ulises Espinoza Nava of the Institute of Engineering. We are grateful for the support of the IDCBIS for their collaboration in the cellular studies.

References

1 N. I. o. B. I. a. B. (NIBIB), Ingeniería de Tejidos y Medicina Regenerativa, https://www.nibib.nih.gov/espanol/temas-cientificos/ingenier%C3%ADa-de-tejidos-y-medicina-regenerativa-0, (accessed March, 2024).
2 X. Li, L. Wang, Y. Fan, Q. Feng, F. Z. Cui and F. Watari, *J. Biomed. Mater. Res. A*, 2013, **101**, 2424–2435.
3 A. Bandyopadhyay, I. Mitra, S. B. Goodman, M. Kumar and S. Bose, *Prog. Mater. Sci.*, 2023, **133**, 101053.
4 K. Elhattab, S. B. Bhaduri and P. Sikder, *Polymers*, 2022, **14**, 1222.
5 E. Salamanca, T.-C. Tsao, H.-W. Hseuh, Y.-F. Wu, C.-S. Choy, C.-K. Lin, Y.-H. Pan, N.-C. Teng, M.-C. Huang and S.-M. Lin, *Front. Mater.*, 2021, **8**, 683706.
6 G. Turnbull, J. Clarke, F. Picard, P. Riches, L. Jia, F. Han, B. Li and W. Shu, *Bioact. Mater.*, 2018, **3**, 278–314.
7 M. Tavakoli, R. Emadi, H. Salehi, S. Labbaf and J. Varshosaz, *Int. J. Biol. Macromol.*, 2023, **253**, 126510.
8 X. Chen, G. Chen, G. Wang, P. Zhu and C. Gao, *Adv. Eng. Mater.*, 2020, **22**, 1901065.
9 R. Donate, M. Monzón, Z. Ortega, L. Wang, V. Ribeiro, D. Pestana, J. M. Oliveira and R. L. Reis, *J. Tissue Eng. Regener. Med.*, 2020, **14**, 272–283.
10 E. Stoleru, T. Zaharescu, E. G. Hitruc, A. Vesel, E. G. Ioanid, A. Coroaba, A. Safrany, G. Pricope, M. Lungu, C. Schick and C. Vasile, *ACS Appl. Mater. Interfaces*, 2016, **8**, 31902–31915.
11 S. Bansal, V. Chauhan, S. Sharma, R. Maheshwari, A. Juyal and S. Raghuvanshi, *Indian J. Orthop.*, 2009, **43**, 234–239.
12 H. Golzar, D. Mohammadrezaei, A. Yadegari, M. Rasoulianboroujeni, M. Hashemi, M. Omidi, F. Yazdian, M. Shalbaf and L. Tayebi, *Composites, Part B*, 2020, **185**, 107749.
13 E. H. Backes, L. de Nóbile Pires, H. S. Selistre-de-Araujo, L. C. Costa, F. R. Passador and L. A. Pessan, *J. Appl. Polym. Sci.*, 2021, **138**, 49759.
14 I. Ayadi and F. B. Ayed, *J. Mech. Behav. Biomed. Mater.*, 2016, **60**, 568–580.
15 X.-J. Shen, S. Yang, J.-X. Shen, J.-L. Ma, Y.-Q. Wu, X.-L. Zeng and S.-Y. Fu, *Ind. Crops Prod.*, 2019, **130**, 571–579.
16 G. Wang, C. He, W. Yang, F. Qi, G. Qian, S. Peng and C. Shuai, *J. Nanomater.*, 2020, **2020**, 5634096.
17 H. Belaid, S. Nagarajan, C. Teyssier, C. Barou, J. Barés, S. Balme, H. Garay, V. Huon, D. Cornu, V. Cavaillès and M. Bechelany, *Mater. Sci. Eng. C*, 2020, **110**, 110595.
18 S. Peng, P. Feng, P. Wu, W. Huang, Y. Yang, W. Guo, C. Gao and C. Shuai, *Sci. Rep.*, 2017, **7**, 46604.
19 A. Sharma, S. Gupta, T. S. Sampathkumar and R. S. Verma, *Biomater. Adv.*, 2022, **134**, 112587.
20 N. Ardjomandi, A. Henrich, J. Huth, C. Klein, E. Schweizer, L. Scheideler, F. Rupp, S. Reinert and D. Alexander, *Biomed. Mater.*, 2015, **10**, 045018.
21 J. S. Heo, H. O. Kim, S. Y. Song, D. H. Lew, Y. Choi and S. Kim, *BioMed Res. Int.*, 2016, **2016**, 8196078.
22 M. Kouhi, M. Fathi, M. P. Prabhakaran, M. Shamanian and S. Ramakrishna, *Appl. Surf. Sci.*, 2018, **457**, 616–625.

23 J. Zhu, Z. Qi, C. Zheng, P. Xue, C. Fu, S. Pan and X. Yang, *J. Nanomater.*, 2020, **2020**, 5892506.
24 S. Midha, K. G. Jain, N. Bhaskar, A. Kaur, S. Rawat, S. Giri, B. Basu and S. Mohanty, *Stem Cells Transl. Med.*, 2021, **10**, 303–319.
25 X. Liu, C. Laurent, Q. Du, L. Targa, G. Cauchois, Y. Chen, X. Wang and N. de Isla, *J. Biomed. Mater. Res. A*, 2018, **106**, 3042–3052.
26 Y. Wang, C. Liu, T. Song, Z. Cao and T. Wang, *Heliyon*, 2024, **10**, e26071.
27 C. Liu, H. M. Wong, K. W. K. Yeung and S. C. Tjong, *Polymers*, 2016, **8**, 287.
28 C. Chen, X. Sun, W. Pan, Y. Hou, R. Liu, X. Jiang and L. Zhang, *ACS Sustain. Chem. Eng.*, 2018, **6**, 3862–3869.
29 A. Sánchez-Cepeda, E. Cedeño, E. Marín, M. C. Pazos, S.-C. Ingrid, E. d. J. Muñoz and R. Vera-Graziano, *RSC Adv.*, 2024, **14**, 3267–3279.
30 Y. Zhao, K.-N. Sun, W.-L. Wang, Y.-X. Wang, X.-L. Sun, Y.-J. Liang, X.-N. Sun and P.-F. Chui, *Ceram. Int.*, 2013, **39**, 7627–7634.
31 K. Yang, J. Wan, S. Zhang, Y. Zhang, S.-T. Lee and Z. Liu, *ACS Nano*, 2010, **5**, 516–522.
32 L. F. Ramos de Valle, *Extrusión de plásticos, Principios básicos*, Limusa S. A. de C. V., México, 2012, pp. 69–70, ISBN 9789681845049.
33 D. E. Juárez Robles, Tesis de Maestría, Universidad Nacional Autónoma de México, México, 2018.
34 P. d. c. t. C. D. A. p. Computadora, **http://www.3dcadportal.com/autodesk-inventor-una-buena-alternativa-para-diseno.html**, 2020.
35 C. S. Lovell, J. M. Fitz-Gerald and C. Park, *J. Polym. Sci., Part B:Polym. Phys.*, 2011, **49**, 1555–1562.
36 A. González González, M. Rivas Santana, P. d. C. Zambrano Robledo and R. Quiza, *MRS Adv.*, 2022, **7**, 1206–1211.
37 M. Schneider, N. Fritzsche, A. Puciul-Malinowska, A. Baliś, A. Mostafa, I. Bald, S. Zapotoczny and A. Taubert, *Polymers*, 2020, **12**, 1711.
38 P. Zhuang, X. Wu, H. Dai, Y. Yao, T. Qiu, Y. Han and S. Li, *Mater. Des.*, 2021, **208**, 109881.
39 L. Jaidev and K. Chatterjee, *Mater. Des.*, 2019, **161**, 44–54.
40 A. Munive-Olarte, J. J. Hidalgo-Moyle, C. Velasquillo, K. Juarez-Moreno and J. D. Mota-Morales, *J. Colloid Interface Sci.*, 2022, **607**, 298–311.
41 M. Gong, Q. Zhao, L. Dai, Y. Li and T. Jiang, *J. Asian Ceram. Soc.*, 2017, **5**, 160–168.
42 M. Ebrahimi, M. G. Botelho and S. V. Dorozhkin, *Mater. Sci. Eng. C*, 2017, **71**, 1293–1312.
43 L. González-Rodríguez, S. Pérez-Davila, R. Lama, M. López-Álvarez, J. Serra, B. Novoa, A. Figueras and P. González, *RSC Adv.*, 2023, **13**, 15947–15959.
44 M. Yashima, A. Sakai, T. Kamiyama and A. Hoshikawa, *J. Solid State Chem.*, 2003, **175**, 272–277.
45 L. Siqueira, F. R. Passador, M. M. Costa, A. O. Lobo and E. Sousa, *Mater. Sci. Eng. C*, 2015, **52**, 135–143.
46 H.-D. Huang, P.-G. Ren, J.-Z. Xu, L. Xu, G.-J. Zhong, B. S. Hsiao and Z.-M. Li, *J. Membr. Sci.*, 2014, **464**, 110–118.
47 S. Jia, D. Yu, Y. Zhu, Z. Wang, L. Chen and L. Fu, *Polymers*, 2017, **9**, 528.
48 R. Baptista, M. Guedes, M. F. C. Pereira, A. Maurício, H. Carrelo and T. Cidade, *Bioprinting*, 2020, **20**, e00096.
49 L. T. Sin, A. R. Rahmat and W. A. W. A. Rahman, in *Polylactic Acid*, ed. L. T. Sin, A. R. Rahmat and W. A. W. A. Rahman, William Andrew Publishing, Oxford, 2013, pp. 177–219, DOI: **10.1016/B978-1-4377-4459-0.00005-6**.
50 C. Medeiros, B. Silva, A. Medeiros, J. Melo and A. Barbosa, *Polym. Bull.*, 2023, **81**, 1–11.
51 D. Wu, P. Isaksson, S. J. Ferguson and C. Persson, *Acta Biomater.*, 2018, **78**, 1–12.
52 L. Feng, G. Gao, P. Huang, X. Wang, C. Zhang, J. Zhang, S. Guo and D. Cui, *Nanoscale Res. Lett.*, 2011, **6**, 551.
53 B. Wang, X. Ye, G. Chen, Y. Zhang, Z. Zeng, C. Liu, Z. Tan and X. Jie, *Front. bioeng. biotechnol.*, 2024, **12**, 1.
54 X. Liu, H. Pan, H. Fu, Q. Fu, N. Rahaman and W. Huang, *Biomed. Mater.*, 2010, **5**, 15005.
55 X. Chen, C. Gao, J. Jiang, Y. Wu, P. Zhu and G. Chen, *Biomed. Mater.*, 2019, **14**, 065003.
56 M. M. S. Mohd Sabee, N. Kamalaldin, B. Yahaya and Z. A. Hamid, *J. Polym. Mater.*, 2016, **33**, 191–200.
57 J. Rydz, W. Sikorska, M. Kyulavska and D. Christova, *Int. J. Mol. Sci.*, 2015, **16**, 564–596.
58 M. E. Berrio, A. Oñate, A. Salas, K. Fernández and M. F. Meléndrez, *Mater. Today Chem.*, 2021, **20**, 100422.
59 M. Tavakoli, R. Emadi, H. Salehi, S. Labbaf and J. Varshosaz, *Int. J. Biol. Macromol.*, 2023, **253**, 126510.
60 T. Liu, B. Li, G. Chen, X. Ye and Y. Zhang, *Int. J. Biol. Macromol.*, 2022, **221**, 371–380.
61 T. Patel, M. Skorupa, M. Skonieczna, R. Turczyn and K. Krukiewicz, *Bioelectrochemistry*, 2023, **152**, 108465.
62 T. I. Croll, A. J. O'Connor, G. W. Stevens and J. J. Cooper-White, *Biomacromolecules*, 2004, **5**, 463–473.
63 C. Kalogirou, O. Höfft, A. Gödde, N. Papadimitriou, P. K. Pandis, C. Argirusis and G. Sourkouni, *J. Polym. Environ.*, 2023, **31**, 345–357.
64 H. Soleymani, M. M. Moghaddam, H. Naderi-Manesh and R. A. Taheri, *Sci. Rep.*, 2024, **14**, 25272.
65 M. S. Kang, S. J. Jeong, S. H. Lee, B. Kim, S. W. Hong, J. H. Lee and D.-W. Han, *Biomater. Res.*, 2021, **25**, 4.
66 S. Bahrami, N. Baheiraei and M. Shahrezaee, *Sci. Rep.*, 2021, **11**, 16783.
67 Y. Hou, W. Wang and P. Bartolo, *Mater. Today Bio*, 2024, **24**, 100886.
68 A. Marrella, P. Giannoni, I. Pulsoni, R. Quarto, R. Raiteri and S. Scaglione, *ACS Appl. Mater. Interfaces*, 2018, **10**, 41978–41985.
69 J.-b. Park, D.-b. Park, J.-h. Lee, S.-j. Yang, J.-e. Lee, J.-K. Park, J.-S. Huh and J.-O. Lim, *Appl. Sci.*, 2022, **12**, 11599.
70 A. □elaru, H. Herman, G. M. Vlăsceanu, S. Dinescu, S. Gharbia, C. Baltă, M. Ro□u, C. V. Mihali, M. Ioni□ă, A. Serafim, H. Iovu, A. Hermenean and M. Costache, *Int. J. Mol. Sci.*, 2022, **23**, 491.
71 C. Wu, L. Xia, P. Han, M. Xu, B. Fang, J. Wang, J. Chang and Y. Xiao, *Carbon*, 2015, **93**, 116–129.

72 J. H. Nam, A. A. Almansoori, O. J. Kwon, Y. K. Seo, B. Kim, Y. K. Kim, J. H. Lee and K. Pang, *J. Periodontal Implant Sci.*, 2023, **53**, 218–232.
73 R. Cabrera-Pérez, M. Monguió-Tortajada, A. Gámez-Valero, R. Rojas-Márquez, F. E. Borràs, S. Roura and J. Vives, *Stem Cell Res. Ther.*, 2019, **10**, 356.
74 J. Li, H. Zeng, Z. Zeng, Y. Zeng and T. Xie, *ACS Biomater. Sci. Eng.*, 2021, **7**, 5363–5396.
75 Q. Fu, E. Saiz, M. N. Rahaman and A. P. Tomsia, *Mater Sci Eng C Mater Biol Appl*, 2011, **31**, 1245–1256.
76 T. Matsubara, K. Kida, A. Yamaguchi, K. Hata, F. Ichida, H. Meguro, H. Aburatani, R. Nishimura and T. Yoneda, *J. Biol. Chem.*, 2008, **283**, 29119–29125.
77 N. AlMuraikhi, S. Binhamdan, H. Alaskar, A. Alotaibi, S. Tareen, M. Muthurangan and M. Alfayez, *Int. J. Mol. Sci.*, 2023, **24**, 7164.
78 M. Wu, Y. Wang, J. Z. Shao, J. Wang, W. Chen and Y. P. Li, *Proc. Natl. Acad. Sci. U. S. A.*, 2017, **114**, 10119–10124.
79 J. Guo, G. Cao, S. Wei, Y. Han and P. Xu, *Heliyon*, 2023, **9**, e21872.
80 Q. Wang, M. Li, T. Cui, R. Wu, F. Guo, M. Fu, Y. Zhu, C. Yang, B. Chen and G. Sun, *Int. J. Mol. Sci.*, 2023, **24**, 2691.
81 M. Wu, L. Zou, L. Jiang, Z. Zhao and J. Liu, *J. Tissue Eng. Regener. Med.*, 2021, **15**, 915–935.
82 G. Lutzweiler, A. Ndreu Halili and N. Engin Vrana, *Pharmaceutics*, 2020, **12**, 602.